ELSEVIER

Journal of Photochemistry and Photobiology A: Chemistry 150 (2002) 187–194

Journal of Photochemistry and Photobiology A:Chemistry

www.elsevier.com/locate/jphotochem

Photochemical formation of nonlinear optical and photorefractive image in polymer layer

A.V. Vannikov [a,*], A.D. Grishina [a], L.Ya. Pereshivko [a], T.V. Krivenko [a], V.V. Savelyev [a], L.I. Kostenko [b], R.W. Rychwalski [c]

[a] *A.N. Frumkin Institute of Electrochemistry, Russian Academy of Science, Leninsky Prospect, 31, 117071 Moscow, Russia*
[b] *Institute of Physico-Organic Chemistry and Coal Chemistry, National Academy of Sciences of Ukraine, R. Luxemburg 70, 340114 Donezk, Ukraine*
[c] *Department of Materials Science and Engineering, Chalmers University of Technology, SE-41296 Göteborg, Sweden*

Received 16 October 2001; received in revised form 18 February 2002; accepted 11 March 2002

Abstract

The paper is devoted to the development of the light-sensitive layers in which the image with nonlinear optical (NLO), photoelectric and photorefractive (PR) properties arises as a result of the photochemical reaction. Layers were obtained by using poly(hydroxyaminoether) (PHAE) containing electron-donor aromatic amino-groups in polymer chains doped with tetrabromomethane as an acceptor. The amino-groups and tetrabromomethane molecules form donor–acceptor complexes the photoexcitation of which induces electron transfer from the donor to the acceptor leading to the synthesis of a colored polycation product which possesses charge carrier photo-generating and NLO properties. Besides, these layers are electron-transporting. This allowed to obtain light-sensitive layers for recording NLO and PR images and pictures.

Keywords: Polymer light-sensitive donor–acceptor layers; Photochemical synthesis; Photoelectric and nonlinear optical properties; Photorefractive image

1. Introduction

Photorefractive (PR) effect in π-conjugated polymer systems has attracted considerable interest because its understanding has led not only to prospects of appreciable technological applications but also to new phenomena, new theoretical concepts, and new materials and devices. In recent years, the main issues have focused on high-performance materials that demonstrate high magnitudes of diffraction efficiency and a net two-beam coupling gain coefficient. Numerous PR polymer composites have been synthesized by using different synthetic approaches, guest matrices, sensitizers, transport agents and electro-optic chromophors. At present, the most efficient materials are host–guest polymer composites of a photoconductive polymer and nonlinear optical (NLO) chromophores [1–5]. But host–guest polymer composites exhibit low stability due to phase separation. The potential advantages of main-chain polymers compared with guest–host and also side-chain systems are as follows. Probability of the formation of dimers and other aggregates in main-chain polymers is far less than in the case of side-chain systems and molecularly doped host–guest polymers. It is known that dimers and aggregates are deep traps for charge carriers therefore impede electron–hole transport. Besides, dipole moments of molecules compensate each other in aggregates and the orientation of these molecules by an external electric field leading to the electro-optic response needed for the PR effect is hampered. But chemical synthesis of polymers combining electron-generating, electron-transporting and NLO units in a main chain is a very complicated task. As an alternative, in the present work for the first time a photochemical synthesis of the similar polymer structure possessing PR properties is demonstrated. Furthermore, the photochemical method affords an opportunity to draw NLO and PR images with UV light from lamp or laser beam on polymer film.

In the present paper, the layers of poly(hydroxyaminoether) (PHAE) with electron–donor aromatic amino-groups (Am) in the main chain $(–R–Am–)_n$ doped with tetrabromomethane (CBr_4) as an acceptor were used

* Corresponding author. Tel.: +7-95-9523-122; fax: +7-95-9520-846.
E-mail address: van@elchem.ac.ru (A.V. Vannikov).

1010-6030/02/$ – see front matter
PII: S1010-6030(02)00143-0

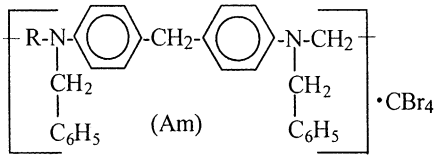

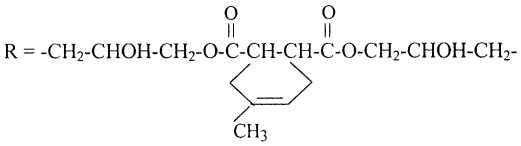

R is a fragment of chain containing ether and hydroxy groups responsible for adhesion, flexibility and other useful properties of the polymer.

The main attention is focused on photoelectric, nonlinear optic and PR properties which appear due to photochemical formation of the polycationic chromophores in main chain PHAE.

2. Experimental

The number–average molecular weight (M_n) of PHAE has been determined by vapor pressure osmometry method. The polymer had $M_n \cong 6000$ and polymerization degree $n \cong 9$. In spite of the low values of M_n the layers of PHAE possess high physico-mechanical characteristics and have the glass transition temperature of about 75 °C. Samples were prepared by dissolving PHAE and CBr_4 in acetone and by casting acetone solution onto glass substrate coated with an conducting film (indium–tin oxide, ITO). After that the layers were dried at 40 °C for 2 h. The dried polymer layers contained 0.8 mol dm^{-3} Am-groups of PHAE and 0.09 mol dm^{-3} CBr_4. The layers were exposed on the whole surface to light of 365 nm wavelength (from Hg-arc lamp) to different exposure doses. To obtain the image, the layer had to be exposed through the suitable mask.

3. Results and discussion

In layer containing PHAE and CBr_4 the donor–acceptor complexes Am·CBr_4 are formed, the concentration of which depends on quantity of the introduced CBr_4. Fig. 1 shows that the PHAE absorption has a long wavelength threshold at 370 nm. Addition of the acceptor CBr_4 shifts this threshold to the region of 500 nm because of the formation of the charge-transfer complex Am·CBr_4 characterized by a broad band peaked at 400 nm. As seen in Fig. 1, under the action of the light at 365 nm there appears an additional band in the long wavelength range between 600 and 700 nm with a maximum at 630 nm. This band is connected with the formation of the polycationic chromophores in the main chain of the PHAE.

Scheme 1 shows that the excitation of the Am·CBr_4 complexes gives rise to electron transfer from amine group to acceptor followed by the transformation of chemical structure of amine group into cationic Michler's hydrol blue (MHB^+)-like chromophore [6,7]. The MHB^+ molar extinction coefficient ε_{max} is 1.47×10^4 dm^3 mol^{-1} cm^{-1} [6,7].

The optical absorbance at 630 nm increases linearly from 0 to 0.6 with increasing exposure dose up to 300 mJ/cm^2

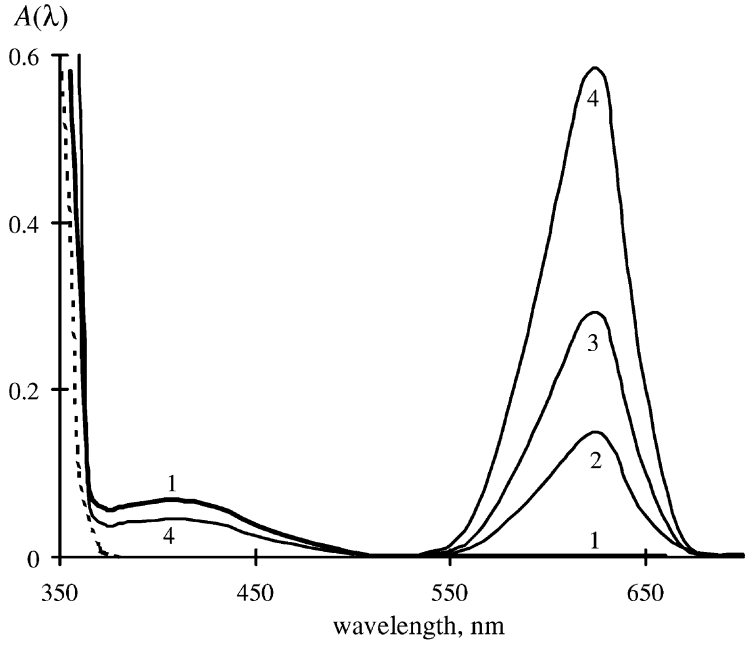

Fig. 1. The absorbance $A(\lambda)$ of PHAE layers undoped (dashed line) and doped with CBr_4 (solid lines). Exposure dose (mJ/cm^2): 0 (1), 75 (2), 150 (3) and 300 (4). Exposing wavelength is 365 nm.

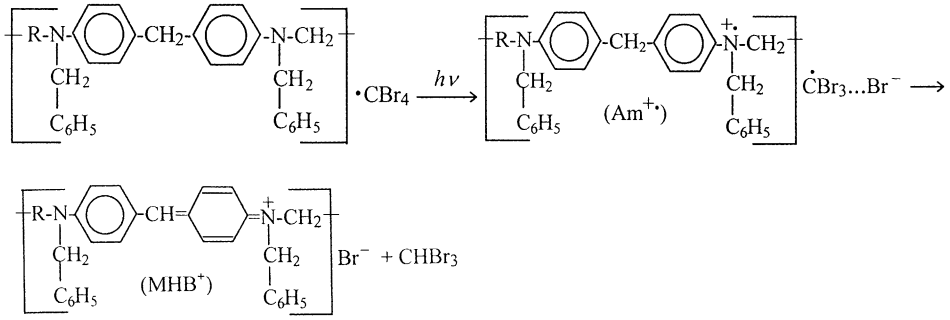

Scheme 1.

(Fig. 1). After exposure the layers were fixed by baking for 2 h at 60 °C. By baking, unreacted CBr_4 was removed and the layer lost light sensitivity. Thus, the exposed areas consisted of the PHAE containing the MHB^+Br^- chromophores in the main chain and the unexposed ones contained only PHAE.

Photo- and dark electric properties. It is well known that the exposed areas of PHAE have photoelectric sensitivity [8,9]. Photoexcitation of MHB^+Br^- in the wavelength range of 600–700 nm induces electron transfer according to the reaction:

$$MHB^+Br^- \xrightarrow{h\nu} (MHB^+Br^-)^* + Am \rightarrow MHB^\bullet Br^- + Am^{\bullet +} \quad (1)$$

followed by the formation of trapped electron ($MHB^\bullet Br^-$) and mobile hole ($Am^{\bullet +}$). The hole transport is a multiple successive electron hopping from the neutral Am-group to the neighbor radical-cation $Am^{\bullet +}$ [10]

$$Am^{\bullet +} + Am \rightarrow Am + Am^{\bullet +} \rightarrow \text{and so on} \quad (2)$$

Hole drift mobility. Hole drift mobility, μ, was measured by a standard time-of-flight (TOF) technique. Samples having a sandwiched electrode configuration were prepared for the TOF measurement. The corresponding solution was cast onto ITO-coated glass. After exposure and fixation of the polymer layer, a charge generating Se layer with a thickness ~0.2 μm and a semitransparent top Au electrode were deposited one after another on the free surface of the layer. Hole–electron pairs were created by a short (10 ns) light pulse of N_2 laser through the Au electrode. The drift mobility was determined from expression $\mu = d/(E_0 t_T)$, where d is the polymer layer thickness, E_0 the applied field, t_T the measured time of the hole transit through the polymer layer.

The temperature and electric field dependencies of the hole drift mobility fit the Gill's equation [9]:

$$\mu = \mu_0 \exp\left[-(\Delta - bE_0^{1/2})\left(\frac{1}{T} - \frac{1}{T_0}\right)\right] \quad (3)$$

with Δ denotes the activation energy, T the temperature, μ_0, b and T_0 are constants. For example, at room temperature for $A(630) = 0.4$ and $E_0 = 50\,V/\mu m$, μ equals to $2.4 \times 10^{-6}\,cm^2/V\,s$, sharply exponentially decreasing with diminishing E_0.

The photo- and dark current measurements. These measurements were carried out using a simple dc current technique with an externally applied electric field $E_0 = 8\,V/\mu m$ and excitation (in the case of photoconductivity) with a Ar–Kr-laser beam, $\lambda = 647$ nm, of the intensity $1.44\,W/cm^2$.

Fig. 2 shows the measured temporal increase of $(j_{ph} + j_d)/j_d$ during exposing by the laser beam and its decay after the laser beam is switched off for the sample having MHB^+ optical absorption $A(647) = 0.08$, thickness 30 μm; j_{ph} and j_d being photo and dark currents, correspondingly. The experimental data in Fig. 2 are well fit with the double exponential function (solid curves)

$$\frac{j_{ph} + j_d}{j_d} = 14 - 9\exp\left(\frac{-t}{24}\right) - 4\exp\left(\frac{-t}{2}\right) \quad (4)$$

for the photocurrent during irradiation by the laser beam and

$$\frac{j_{ph} + j_d}{j_d} = 1 + 9\exp\left[-\frac{t - t_1}{24}\right] + 4\exp\left[-\frac{t - t_1}{2}\right] \quad (5)$$

for the current decay after the laser beam is switched off at t_1. Fig. 3 shows the dependence of j_{phm}/j_d and j_d on $A(647)$, where j_{phm} is the maximal photocurrent.

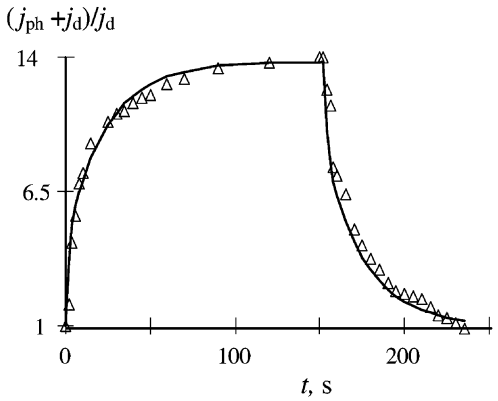

Fig. 2. Photocurrent dependence on time for the sample with $A(647) = 0.08$ and thickness $d = 30$ μm. At $t = 0$ laser beam is switched on, at $t_1 = 150$ s it is switched off.

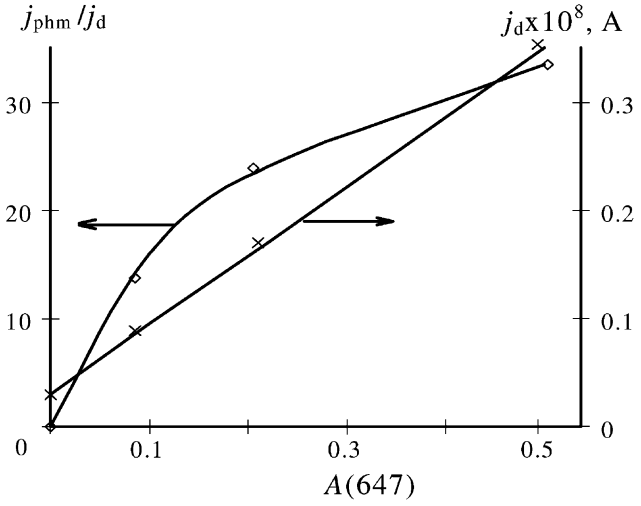

Fig. 3. Dependence of dark current and steady-state photo-current on $A(647)$.

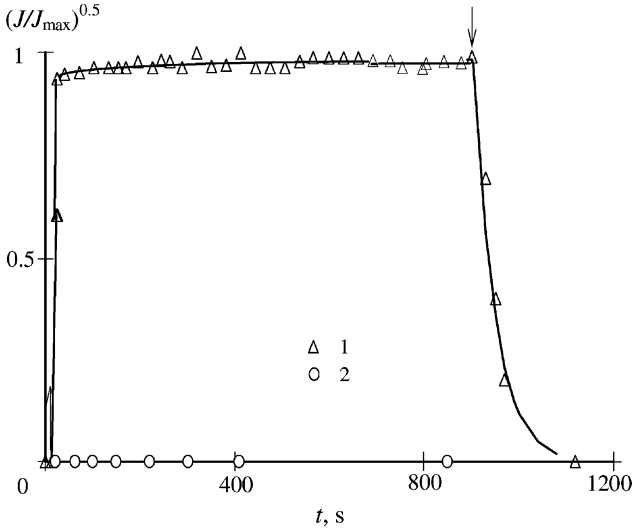

Fig. 4. Time dependence of the relative SH intensity, $(J/J_{max})^{0.5}$, for the exposed (1) and the unexposed (2) areas. Corona discharge is switched on and off (arrow up and down).

Thus, an internal space–charge electric field E_{sc} formation should be expected when a fringe pattern is created by two intersecting laser beams in the presence of the external field E_0.

Second harmonic generation (*SHG*). Photochemical formation of the MHB^+Br^- chromophores leads to a manifestation of NLO properties, namely SHG [11]. The samples were irradiated by pulses of Nd:YAG laser having a fundamental wavelength of 1064 nm, beam diameter of 0.3 cm, energy of ~50 mJ per pulse and duration of 10 ns. A negative surface potential U forming dc electric field E_0 across the sample was applied to the polymer layer surface by the corona discharge method. A steel wire suspended 1 cm away from the polymer surface was biased at a high negative voltage, $V = 4$ kV. The ITO was used as a grounding electrode. The high voltage ionized air around the wire. Resulting ions deposited on polymer produced a surface charge. The SH intensity (J) (i.e. J at the wavelength of 532 nm) generated by polymer layer was measured using a photo-amplifier and a digital voltmeter. The digital voltmeter indications (in mV) were proportional to the intensity J, where $J^{0.5} \propto \chi^{(2)}$ and $\chi^{(2)}$ is the second-order macroscopic polarizability. The digital voltmeter indications were registered after each laser pulse. The dark decay of the surface potential for the same samples was measured with a noncontacting capacitively coupled probe and amplifier in parallel experiments [12].

As seen in Fig. 4, the SHG signal is characteristic of the exposed areas of the layer and it is absent on the unexposed ones, for the same layer. The SHG signal appears when the corona discharge is switched on and it disappears when the corona discharge is switched off. The $(J/J_{max})^{0.5}$ and surface potential (U/U_{max}) decay curves after switching off the corona discharge completely coincide and can be represented by the common equation:

$$\left(\frac{J}{J_{max}}\right)^{0.5} = \left(\frac{U}{U_{max}}\right) = \exp\left(-\frac{t}{\tau_e}\right) \quad (6)$$

where the time constant $\tau_e = 45$ s. Hence, the dc electric-field-induced-SH generation (EFISHG) takes place. The SH intensity linearly increases with increasing the MHB^+Br^- concentration (that is with increasing $A(647)$ in Fig. 1) and comes near to $(\chi^{(2)} + \chi^{(3)}E_0) \approx 2$ pm/V at $A(647) = 0.6$ (here $\chi^{(3)}$ is the third-order macroscopic polarizability). This value is obtained by comparing SH signals for MHB^+Br^- and PMMA doped with noncentrosymmetrical chromophore Disperse Orange 3 at concentration 3×10^{20} cm^{-3} for which as known [13] $(\chi^{(2)} + \chi^{(3)}E_0) = 11.6$ pm/V.

In order to understand the mechanism of SHG, the dipole moments of the MHB^+ fragment in ground and first excited states were estimated using the semiempirical PM3 method [11]. The computing was performed with the HyperChem program (Hypercube). The MHB^+ is a bond-equivalent symmetrical fragment. In accordance with a known notion [14], we optimized first the structure geometry of MHB^+Br^- consisting of the conjugated cation and the point counter anion and then the counter anion was withdrawn [11]. The optimized structure corresponds to a minimal possible distance between MHB^+ and Br^-. In this nonequilibrium geometry of MHB^+, the estimated dipole moments for the MHB^+ ground state (μ_g) and first excited state (μ_e) are equal to 7.5 D and 1.5 D, respectively. Thus, the Br^- counter anion induces the bond-length alternation of the MHB^+ cation and hence produces the molecular second-order nonlinear behavior. Indeed, the second-order macroscopic polarizability is defined by equation $\chi^{(2)} = NE_0[(\beta\mu_g/5kT) + \gamma]$, where N is the number of MHB^+ chromophores in unit volume, $\beta \sim \mu_{ge}^2(\mu_e - \mu_g)/(h\nu_{ge})^2$ and γ are the second- and third-order molecular polarizabilities accordingly, μ_{ge} and $h\nu_{ge}$ are the transitional dipole moment and transition energy, respectively, between the ground state (g) and first allowed excited

state (e). In this case, the refractive index modulation creating a phase grating can be represented by the expression:

$$\Delta n = \frac{2\pi E_{sc}(\chi^{(2)} + \chi^{(3)} E_0)}{n}$$

During poling procedure two major contributions can be considered for the formation of polar structure. One is the change in orientation of chromophore MHB^+ as generally observed in the nonionic poled polymer systems. The other is the change in the relative position of Br^- to MHB^+. However, although the change of the distance between MHB^+ and Br^- invokes the change of the dipole moments, noncentrosymmetric macroscopic structure does not appear with that. So, we believe that the second-order polarizability $\chi^{(2)}$ is mainly coupled to the orientation of dipole chromophore MHB^+ in a strong electric field. The orientation manifested itself in the decrease of optical absorption by several per cent at 647 nm.

Thus, the polymer layer obtained by photochemical modification of the PHAE-CBr_4 (Scheme 1) possesses photoelectric and NLO properties which are necessary for the PR effect.

PR effect. Ar–Kr-laser, $\lambda = 647$ nm, and the two-beam coupling technique were used to characterize the PR effect. As seen in Fig. 5, two coherent writing *p*-polarized beams were overlapped in the photochemically modified polymer layer to create a fringe pattern (dashed lines) and phase-shifted refractive index grating Δn (solid lines). In order to provide the holes drift and also to orient the initially randomly distributed MHB^+ and to obtain macroscopic second-order properties an external electric field E_0 was applied. In these experiments, two electrode structures were used: (1) glass slide/ITO as a grounded electrode/polymer layer on the free surface of which a uniform negative charge forming negative surface potential was deposited by the above-mentioned corona discharge technique and (2) the structure in which the polymer layer was sandwiched between two ITO-coated glass slides is shown in Fig. 5. For the first variant structures, the applied electric field was equal to $E_0 = 8$ V/μm. For the shown in Fig. 5 second variant, the electric field changed and reached more than 50 V/μm.

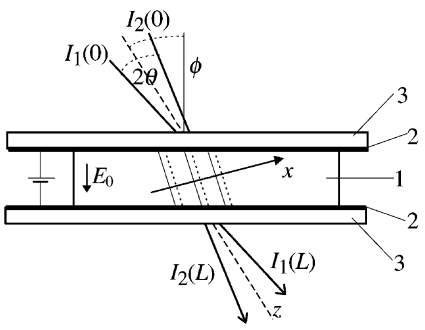

Fig. 5. Experimental setup for two-beam coupling (see text). Polymer layer (1), electrodes from conducting ITO films (2) and glass substrates (3).

Fig. 5 shows the geometry of the two-beam coupling experiment where the $I_1(0)$ and $I_2(0)$ are input intensities of the pumping and signal beams, accordingly. $I_1(L)$ and $I_2(L)$ are their output intensities; θ is angle between bisector and the beam ($2\theta = 15°$), $\phi = 45°$ is the title angle. The concentrations of the photochemically formed MHB^+ estimated by the formula $C = A(630)/\varepsilon_{max} d$ ranged between 2×10^{-3} and 3.8×10^{-2} mol dm^{-3}.

The kinetics of the two-beam coupling are given in Figs. 6 and 7. The results for first variant structure ($E_0 = 8$ V/μm) containing the polymer layer with $A(647) = 0.4$ and $d = 7.4$ μm are given in Fig. 6. The results of three separate experiments are shown. In the first experiment, the beam 1 intensity (curves 1) was measured before and after the switching on of beam 2 in moment $t = 0$ s (arrow up) and after it was switched off at $t = 50$ s (arrow down) for $I_1(0) = 720$ mW/cm^2 and a beam ratio before the sample $\beta = I_1(0)/I_2(0) = 1$. Fig. 6 gives the normalized intensity $I_1(L)/I_1(L)_{t=0}$ where $I_1(L)_{t=0}$ and $I_1(L)$ are the beam 1 output intensities without the beam 2 (in moment $t = 0$) and after its switching on, respectively. In the second and third experiments the same procedure was repeated for beam 2 for $\beta = 1$ (curve 2) and after decrease of the beam 2 intensity to value $I_2(0) = 164$ mW/cm^2 corresponding $\beta = 4.4$ (curve 3). The normalized intensities give the beam-coupling ratio $\gamma = I_2(L)/I_2(L)_{t=0}$.

It is shown in Fig. 6 that the experimental data are well fitted with the expressions:

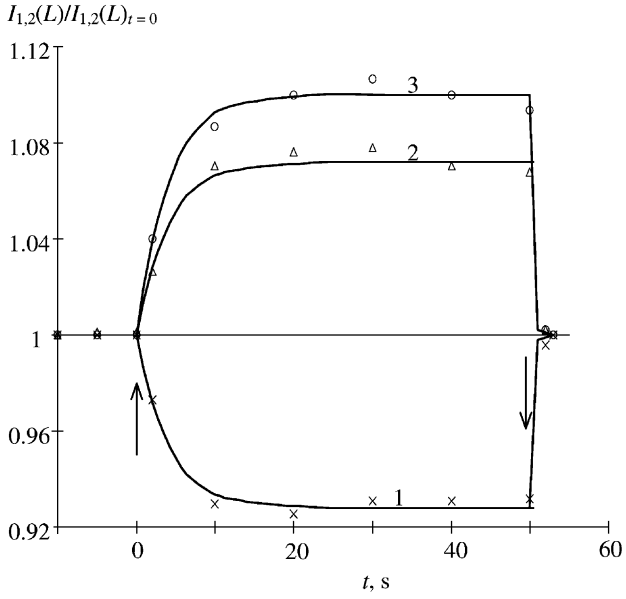

Fig. 6. The normalized curves of the two-beam coupling for sample having $A(647) = 0.4$ and $d = 7.4$ μm. $E_0 = 8$ V/μm, $I_1(0) = 720$ mW/cm^2. The output intensity of the beam 1, $I_1(L)$ (curve 1) was measured as beam 2 is switched on (arrow up) and off (arrow down). Then the intensities of the beam 2 $I_2(L)$ were measured as beam 1 is switched on and off at $\beta = 1$ (curve 2) and 4.4 (curve 3). (Each curve was measured on new area of the exposed layer.) $I_1(L)_{t=0}$ and $I_2(L)_{t=0}$ are intensities in the absence of beams 2 and 1, respectively (at $t = 0$).

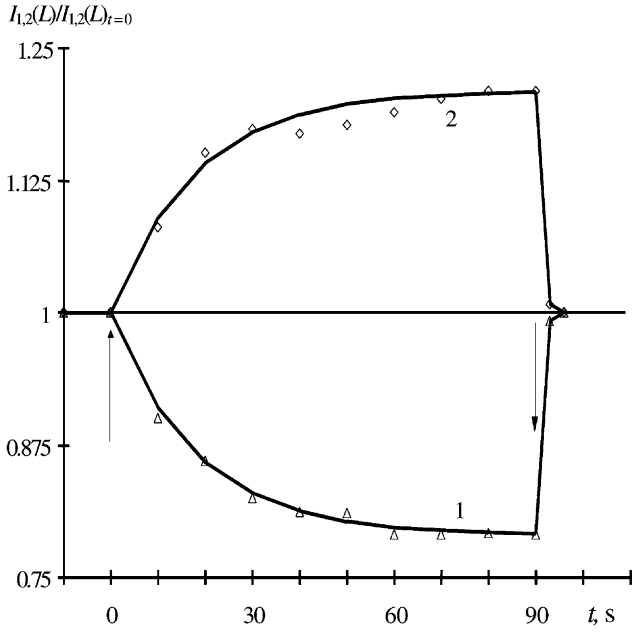

Fig. 7. The normalized curves of the two-beam coupling for sample having $A(647) = 0.055$ and $d = 19.4\,\mu m$. $E_0 = 26\,V/\mu m$, $I_1(0) = 78\,mW/cm^2$ and $\beta = 1$.

$$\frac{I_1(L)}{I_1(L)_{t=0}} = 1 - 0.072\left\{1 - \exp\left[-\left(\frac{t}{\tau}\right)\right]\right\}$$

(for solid curve 1, $\beta = 1$),

$$\frac{I_2(L)}{I_2(L)_{t=0}} = 1 + 0.072\left\{1 - \exp\left[-\left(\frac{t}{\tau}\right)\right]\right\}$$

(for solid curve 2, $\beta = 1$)

$$\frac{I_2(L)}{I_2(L)_{t=0}} = 1 + 0.1\left\{1 - \exp\left[-\left(\frac{t}{\tau}\right)\right]\right\}$$

(for solid curve 3, $\beta = 4.4$).

From these expressions it follows that after achieving steady state of the beam intensity, the saturation amplification factors $\gamma_0 = I_2(L)/I_2(L)_{t=0}$ were equal to 1.072 and 1.1 for $\beta = 1$ and 4.4, respectively. Here $\tau = 4\,s$ is the grating buildup time (response time) constant.

Fig. 7 shows energy transfer in the results of two-beam coupling obtained at $E_0 = 26\,V/\mu m$ using the cell shown in Fig. 5 for the photochemically modified polymer layer with $A(647) = 0.055$ and thickness $d = 19.4\,\mu m$ and hence having the MHB^+ concentration equal to $2 \times 10^{-3}\,mol\,dm^{-3}$ ($\chi^{(2)} + \chi^{(3)}E_0$) about 0.2 pm/V and absorption coefficient $\alpha = A(647)/(d \log e) = 65.5\,cm^{-1}$. The input intensity of each writing beam was $78\,mW/cm^2$, i.e. a ratio of the beam intensities before the sample $\beta = 1$. The beam 1 output intensity $I_1(L)$ was measured as beam 2 was switched on in the moment $t = 0$ (arrow up) and switched off at $t = 90\,s$ (arrow down) giving a normalized intensity curve $I_1(L)/I_1(L)_{t=0}$ (1). Then the same procedure was repeated for beam 2 giving the beam-coupling ratio $\gamma = I_2(L)/I_2(L)_{t=0}$ (2). As seen in Fig. 6 for $\beta = 1$ and Fig. 7, as the refractive index grating Δn is written the intensity of beam 1 decreases and the intensity of beam 2 increases by approximately the same quantity indicating a shift between the refraction index grating and the light intensity grating.

The solid lines in Fig. 7 correspond to the equations:

$$\frac{I_1(L)}{I_1(L)_{(t=0)}} = 1 - 0.22\left[1 - \exp\left(-\frac{t}{\tau}\right)\right] \quad (7)$$

$$\gamma = \frac{I_2(L)}{I_2(L)_{(t=0)}} = 1 + 0.22\left[1 - \exp\left(-\frac{t}{\tau}\right)\right] \quad (8)$$

Here response time constant $\tau = 19\,s$, the saturation value $\gamma_0 = 1.22$.

The curves analogous to 1 and 2 in Fig. 6 were measured at different $A(647)$ and β, $I_1(0) = 720\,mW/cm^2$ and at the electric field $E_0 = 8\,V/\mu m$ applied by the corona discharge technique. In Table 1 the PR properties are summarized. Experimental conditions, namely, $A(647)$ and the sample thickness d are given in columns 1 and 2. Column 3 represents the product $\alpha L = A(647)/(\cos(\phi - \theta) \log e)$, where $L = d/\cos(\phi - \theta) = d/0.79$ is the optical path for the beam with gain. The value of β also as the measured saturation value γ_0 and response time are shown in columns 4, 5 and 6. The two-beam coupling gain coefficient Γ is given by [1]

$$\Gamma L = [\ln(\gamma_0\beta) - \ln(1 + \beta - \gamma_0)] \quad (9)$$

Columns 7 and 8 show the ΓL and Γ values. The saturated refractive index modulation and diffraction efficiency that are estimated according to the formulae $\Delta n = \Gamma\lambda/4\pi$ ($\lambda = 647\,nm$) and $\eta = \sin^2(\Gamma L/2)$ [15] are shown in columns 9 and 10, respectively. As seen in Table 1, the gain Γ and

Table 1
PR characteristics of the studied layers $I_1(0) = 720\,mW/cm^2$, $E_0 = 8\,V/\mu m$

$A(647)$	d (μm)	αL	β	γ_0	τ (s)	ΓL	Γ (cm^{-1})	Δn	η (%)
0.08	30	0.23	1	1.041	24	0.082	21.7	1.1×10^{-4}	0.17
0.08	30	0.23	2.36	1.07	24	0.098	26	1.3×10^{-4}	0.24
0.2	30	0.59	1	1.05		0.100	26.4	1.4×10^{-4}	0.25
0.2	30	0.59	4.24	1.15		0.176	46.5	2.4×10^{-4}	0.77
0.4	7.4	1.17	1	1.072	4	0.120	128.6	6.5×10^{-4}	0.5
0.4	7.4	1.17	4.4	1.1	4	0.118	126.5	6.5×10^{-4}	0.35
0.4	7.4	1.17	12	1.15	4	0.152	163	8.5×10^{-4}	0.58
0.4	7.4	1.17	22	1.32	4	0.292	313	1.6×10^{-3}	2.1

Table 2
PR characteristics for photochemically modified layer with thickness 9.7 μm and $A(647) = 0.05$ ($\alpha = 116\,cm^{-1}$), $\beta = 1$

E_0 (V/μm)	γ_0	τ (s)	ΓL	Γ (cm^{-1})	$\Gamma - \alpha$ (cm^{-1})	η (%)	Δn	S (cm^2/J)	S' (cm^2/J)
10.3	1.04	23	0.08	63	−67	0.09	3.2×10^{-4}	0.0001	0.0005
20.6	1.08	22	0.16	131	15	0.64	6.7×10^{-4}	0.00018	0.001
30.9	1.085	20	0.17	140	24	0.73	7.2×10^{-4}	0.00020	0.0012
51.5	1.14	19	0.28	231	115	2	1.2×10^{-3}	0.00033	0.002

hence η and Δn increases with growth of $A(647)$ and β. The ratio $\gamma_0 = 1.32$, $\Gamma = 313\,cm^{-1}$, $\eta = 2.1\%$ and $\Delta n = 1.6 \times 10^{-3}$ is obtained for the sample having $A(647) = 0.4$ and $d = 7.4\,\mu m$ when the intensity of beam 2 is decreased to value $I_2(0) = 32.7\,mW/cm^2$ corresponding $\beta = 22$.

As given in Table 1, for the sample with $A(647) = 0.08$ and $d = 30\,\mu m$ having MHB^+ concentration about 1.8×10^{-3} mol dm^{-3}, the response time constant at the intensities of both beams 720 mW/cm^2 is equal to 24 s and within the experimental error agrees with the above-mentioned slow time constant of the photocurrent for the same sample (Eqs. (4) and (5)). Therefore, the transport and capture of charge carriers is the factor limiting PR speed in these materials. As it is shown in Tables 2 and 3 for the layers with $A(647) = 0.05$, $d = 9.7$ and 19.4 μm, almost the same response time constants (19–24 s) were measured when the input beam intensities were decreased by factor of 9.2 (to $I_1(0) = I_2(0) = 78\,mW/cm^2$). Hence, the warming up contribution in the kinetic curves Figs. 6 and 7 is absent. Fig. 6 and Table 1 show that the response time constants are reduced to $\tau = 4$ s when the layer with $A(647) = 0.4$ having the MHB^+ concentration 3.8×10^{-2} mol dm^{-3} is used. The reduction from 24 to 4 s at the same intensities $I_1(0) = I_2(0) = 720\,mW/cm^2$ perhaps is determined by 20-fold increase of the concentration of the charge-generating centers MHB^+ taking part in photo-process (1). Unfortunately, the corona discharge technique does not allow us to produce electric field higher than 8 V/μm [16]. Therefore, the product ΓL is less than αL under such conditions (Table 1).

Net internal gain ($\Gamma > \alpha$) was achieved on the composites with lower α and higher E_0. Moderate electric fields E_0 were applied to the samples composed of the polymer material (exposed and fixed) sandwiched between two glass plates coated with ITO (Fig. 5).

Represented in Table 2 results were obtained for the photochemically modified layer with thickness 9.7 μm, $A(647) = 0.05$ and hence having the MHB^+ concentration equal to 3.4×10^{-3} mol dm^{-3}, absorption coefficient α equal to $116\,cm^{-1}$ ($\chi^{(2)} + \chi^{(3)} E_0$) about 0.3 pm/V. These data were obtained at $\beta = 1$ and the intensity of each writing beam equal to $78\,mW/cm^2$. The two curves analogous to those of 1 and 2 in Fig. 7 were certainly measured at each value of E_0. The decrease of beam 1 intensity and the beam 2 amplification on the same value is the evidence of the PR origin of the effect. As given in Table 2, the growth E_0 from 10.3 to 51.5 V/μm increases γ_0 from 1.04 to 1.14, hence ΓL from 0.06 to 0.28 (formula (9)) and the gain coefficient Γ from 63 to $231\,cm^{-1}$. The net internal gain is achieved when the applied electric field E_0 exceeds 10 V/μm. For example, the gain coefficient $\Gamma = 231\,cm^{-1}$ at $E_0 = 51.5$ V/μm exceeds the absorption coefficient $\alpha \approx 116\,cm^{-1}$ and a net internal gain $\Gamma - \alpha = 115\,cm^{-1}$.

Table 2 also contains the grating buildup time τ, the values of η% and Δn estimated on the pre-cited formulae and also the PR sensitivities $S = \Delta n / I\tau$ and $S' = \Delta n / I'\tau$ or refractive index change per unit incident fluence and per unit absorbed energy, respectively, i.e. $I = I_1 + I_2 = 0.156\,W/cm^2$; $I' = 0.078(1 - 10^{-A_1}) + 0.078(1 - 10^{-A_2})\tau$, where $A_1 = A(647)L_1/d$, $A_2 = A(647)/\cos(\phi - \theta)$ and $L_1 = d/\cos(\phi + \theta)$ is the optical paths for beam 1.

The higher values $\Gamma - \alpha$ were obtained on the layer with thickness 19.4 μm and $A(647) = 0.055$ having the MHB^+ concentration equal to 2×10^{-3} mol dm^{-3} ($\chi^{(2)} + \chi^{(3)} E_0$) about 0.2 pm/V and $\alpha = 65.5\,cm^{-1}$. Table 3 gives data measured at $I_1(0) = I_2(0) = 78\,mW/cm^2$. As seen, the growth E_0 from 5.15 to 26 V/μm increases γ_0 from 1.06 to 1.22 (Fig. 7, Eqs. (7) and (8)), hence ΓL from 0.12 to 0.44 and the gain coefficient from 49.1 to $183\,cm^{-1}$. Thus, the gain coefficient $\Gamma = 183\,cm^{-1}$ at $E_0 = 26$ V/μm exceeds the absorption coefficient $\alpha = 65.5\,cm^{-1}$ and the net internal gain is about $\Gamma - \alpha \approx 117\,cm^{-1}$.

The value of $\Gamma - \alpha = 188\,cm^{-1}$ at $E_0 > 100$ V/μm and $\Gamma \sim 0$ at $E_0 < 30$ V/μm were reported for the plasticized PVK-based composite for $\beta = 1$ [17]. The maximal difference $\Gamma - \alpha = 207\,cm^{-1}$ at an electric field of 90 V/μm was achieved also in the PVK-based layers [3]. The

Table 3
PR characteristics for photochemically modified layer with thickness 19.4 μm and $A(647) = 0.05$ ($\alpha = 65.5\,cm^{-1}$), $\beta = 1$

E_0 (V/μm)	γ_0	τ (s)	ΓL	Γ (cm^{-1})	$\Gamma - \alpha$ (cm^{-1})	η (%)	Δn	S (cm^2/J)	S' (cm^2/J)
5.2	1.06	24	0.12	49.1	−16.4	0.36	2.5×10^{-4}	0.00007	0.0004
10.3	1.09	23	0.184	75.5	10	0.85	4×10^{-4}	0.00011	0.00066
15.5	1.13	21	0.26	107	41.5	1.7	5×10^{-4}	0.00015	0.001
26	1.22	19	0.45	183	117.5	5	9.5×10^{-4}	0.00032	0.0019

net gain was observed for E_0 above 35 V/μm and achieved $\Gamma - \alpha = 107\,\mathrm{cm}^{-1}$ at $E_0 = 60$ V/μm and $\beta = 1$ for polysiloxane doped by the low molecular species providing both charge-transport and NLO properties [5]. So, the consideration of the PR data evidences that the photochemically modified layers based on PHAE and the best well-known PR polymer materials have similar PR characteristics.

4. Conclusions

Thus, we have shown for the first time that the photochemical method may be used to obtain the layers having PR properties that are comparable with those of well known polymer PR composites. Novel NLO materials and method of their preparation presented in this paper can be characterized by the following attractive possibilities to: (a) uninterruptedly change the concentration of the NLO and charge-generating sites (MHB^+Br^-), (b) simultaneously have transporting (Am), NLO and charge-generating (MHB^+Br^-) sites in main polymer chains, (c) form a photographic image exhibiting the PR and NLO properties in the polymer layer using the photochemical reaction (Scheme 1), (d) to sensitize the PR sensitivity towards the IR range.

Acknowledgements

This work was supported by a grant from Royal Swedish Academy of Science, a grant from International Science and Technology Center (project no. 2207) and the Russian Foundation for Basic Research (project no. 02-03-33052).

References

[1] W.E. Moerner, S.M. Silence, Chem. Rev. 94 (1994) 127.
[2] R.L. Sutherland, Handbook of Nonlinear Optics. Marcel Dekker, New York, 1996, 685 pp. (Chapters 6 and 7).
[3] B. Kippelen, K. Meerholz, N. Peyghambarian, in: H.S. Nalwa, S. Miyata (Eds.), Nonlinear Optics of Ordanic Molecules and Polymers, CRC Press, Boca Raton, 1997, p. 465 (Chapter 8).
[4] E. Mecher, R. Bittner, C. Bräuchle, K. Meerholz, Synth. Met. 102 (1999) 993.
[5] S. Wu, F. Zeng, F. Li, J. Li, React. Funct. Polym. 46 (2001) 225.
[6] A.Yu. Kryukov, A.V. Vannikov, A.V. Anikeev, L.I. Kostenko, Chem. Mater. 4 (1992) 803.
[7] A.V. Vannikov, A.D. Grishina, M.G. Tedoradze, L.I. Kostenko, A.V. Anikeev, I.V. Koblik, J. Mater. Chem. 3 (1993) 761.
[8] A.Yu. Kryukov, A.V. Vannikov, A.A. Pakhratdinov, A.V. Anikeev, L.I. Kostenko, Chem. Mater. 4 (1992) 72.
[9] A.V. Vannikov, in: Proceedings of the ICTS'94: The Physical and Chemistry of Imaging Systems, IS&T's 47 Annual Conference. Final Program and Advance Printing of Papers, 1994, p. 783.
[10] P.M. Borsenberger, D.S. Weiss, Organic Photoreceptors for Xerography, Marcel Dekker, New York, 1998, 768 pp.
[11] A.D. Grishina, L.Ya. Pereshivko, T.V. Krivenko, V.V. Savelyev, E.I. Mal'tsev, A.V. Vannikov, in: M. Eich, M.G. Kuzyk (Eds.), Proceedings of SPIE, Organic Nonlinear Optical Materials, Vol. 3796, 1999, p. 308.
[12] A.D. Grishina, L.Ya. Pereshivko, T.V. Krivenko, V.V. Savel'ev, J. Vernel, R.W. Rychwalski, A.V. Vannikov, Polymer 42 (2001) 4837.
[13] D.M. Burland, R.D. Miller, C.A. Walsh, Chem. Rev. 94 (1994) 31.
[14] C.B. Gorman, S.R. Marder, Proc. Natl. Acad. Sci. USA 90 (1993) 11297.
[15] D.L. Staebler, J.J. Amodei, J. Appl. Phys. 43 (1972) 1042.
[16] A.V. Vannikov, A.D. Grishina, L.Ya. Pereshivko, T.V. Krivenko, V.V. Savelyev, L.I. Kostenko, R.W. Rychwalski, Polym. Sci., Ser. A 43 (2001) 599.
[17] A. Grunnet-Jepsen, C.L. Thompson, R.J. Twieg, W.E. Moerner, Appl. Phys. Lett. 70 (1997) 1515.